Mechanical Systems and Signal Processing 132 (2019) 457–470

Contents lists available at ScienceDirect

Mechanical Systems and Signal Processing

journal homepage: www.elsevier.com/locate/ymssp

Nonlinear positive position feedback control for mitigation of nonlinear vibrations

G. Zhao [a,*], A. Paknejad [a,*], G. Raze [b], A. Deraemaeker [c], G. Kerschen [b], C. Collette [a,b]

[a] Université Libre de Bruxelles, Department of Bio-, Electro- and Mechanical Systems, Precision Mechatronics Laboratory, 50, F.D. Roosevelt Av, B-1050 Brussels, Belgium
[b] University of Liège, Department of Aerospace and Mechanical Engineering, Allée de la Découverte 9, B-4000 Liège, Belgium
[c] Université Libre de Bruxelles, Building Architecture & Town Planning (BATir), 50, F.D. Roosevelt Av, B-1050 Brussels, Belgium

ARTICLE INFO

Article history:
Received 30 April 2019
Received in revised form 28 June 2019
Accepted 4 July 2019
Available online 15 July 2019

Keywords:
Nonlinearity
$\mathcal{H}_\infty$ optimisation
Positive position feedback
Harmonic balance
Duffing oscillator

ABSTRACT

This paper investigates the potential of using a nonlinear positive position feedback controller for vibration mitigation of a Duffing oscillator. The proposed controller is designed based on the principle of similarity which states that anti-vibration devices should be governed by the same equations as those of the host structure. Closed-form expressions for the $\mathcal{H}_\infty$ optimal control parameters that minimise the maximal response of the structure are firstly derived for the linear positive position feedback controller and then extended to the nonlinear counterpart. The harmonic balance method is employed to approximate the analytical solutions. Both numerical simulations and experimental validations are performed to demonstrate the proposed control strategy.

1. Introduction

Controlling nonlinear structural vibrations is becoming increasingly important in a number of engineering applications such as aerospace, medicine and robotics, wherein lightweight materials are considered in the construction of systems in order to meet the increasing demand for fuel efficiency or smaller actuators [1,2]. However, this will naturally lead to the fact that the resonances are lightly damped and to the presence of geometrical nonlinearities resulting from large deformations. The resulting unwanted nonlinear vibrations thus become the main concern, limiting the success of these applications. One key characteristic of nonlinear vibrations is their frequency-energy dependence which means that the frequency of the nonlinear oscillations depends intrinsically on the motion amplitudes [3]. As a consequence, the mature linear damping-enhanced approaches based on the superposition principle such as tuned mass dampers (TMD) and piezoelectric shunting [4–6] (passive solutions) or direct velocity feedback, integral acceleration and force feedback controllers [7–10] (active solutions) are no longer effective in the presence of strong nonlinearities. In order to recover their control effectiveness for a large range of excitation levels, mechanisms that can deliver nonlinear reacting forces should be included in these linear approaches. For example, Agnes [11] suggested to integrate a positive or negative cubic spring into a linear vibration absorber for compensating the softening (hardening) nonlinear effect of the primary systems. Febbo and Machado [12] explored the potential of using a nonlinear absorber with a saturation nonlinearity for vibration mitigation of a nonlinear primary oscillator possessing a cubic stiffness. Habib et al. [13], Detroux et al. [14] and Habib and Kerschen [15] stated that nonlinear

* Corresponding authors.
E-mail addresses: guoying.zhao@ulb.ac.be (G. Zhao), ahmad.paknejad@ulb.ac.be (A. Paknejad).

https://doi.org/10.1016/j.ymssp.2019.07.005
0888-3270/

vibration absorbers can be designed as a mirror of the primary structures i.e. nonlinear vibration absorbers should possess the same nonlinearities as those in the primary systems. This design principle is also referred to as the principle of similarity. It was reported that nonlinear primary systems attached with nonlinear vibration absorbers designed based on the principle of similarity behave in a similar fashion as their linear counterpart. Although this concept is promising, it may become cumbersome and expensive to realise them in practice using passive means for complex nonlinear primary systems.

On the other hand, in an active approach it is attempted to introduce the desired nonlinear control forces using sensors and actuators. This may yield a nonlinear anti-vibration system that is less complex. Various types of active controllers have been investigated for vibration attenuation of nonlinear systems [16–25]. Among them, linear positive position feedback (LPPF) and nonlinear positive position feedback (NPPF) controllers are found to be particularly effective if they are aimed to damp one particular structural vibration mode. This type of controller is implemented by feeding the structural position directly to a linear or nonlinear compensator, whose output is then fed through a fixed gain positively back to drive the actuator. In this context, they would be well suited for the applications where piezoelectric sensors and actuators are employed for vibration damping. This is because the voltage from the sensor is proportional to the strain of the attached structure, which can be directly measured to drive the strain-based piezoelectric actuators. Warminski et al. [21] compared the control performance of a LPPF controller with three other controllers, namely proportional position feedback, cubic position feedback and nonlinear saturation feedback, for suppression of nonlinear composite beam vibrations. It was found that the LPPF controller is only effective for weakly nonlinear systems and the nonlinear saturation controller was concluded to be superior for the nonlinear primary structure under consideration. The performance of the LPPF controller was also investigated in [22], but on a four-degree-of-freedom system with cubic nonlinearities. El-Ganaini et al. [23] studied a nonlinear positive position feedback controller for vibration suppression of a nonlinear system where both cubic and inertial nonlinearities are present. This NPPF controller can be seen as an extension of a LPPF controller where a cubic nonlinear term is added to the linear second order resonant compensator. Omidi and Mahmoodi [24,26] proposed to include an additional first-order low pass filter in parallel to the NPPF controller aiming to enhance the control performance. Although the feasibility of using active means for mitigation of nonlinear vibrations has been successfully demonstrated in the aforementioned studies, limited investigation on the optimisation of these controllers exists.

This study is focused on the optimisation of the described NPPF controller for vibration suppression of a Duffing oscillator and on its experimental validation. The Duffing oscillator is defined as a forced and damped harmonic oscillator with a cubic nonlinearity in the restoring force [27,28]. Although it exhibits a simple form, a variety of physical examples can be dynamically characterised by the Duffing equation such as pendulum dynamics [29], beam buckling [30], cable dynamics [31] and nonlinear isolators [32,33]. Using the NPPF controller for vibration mitigation of a Duffing oscillator can be considered as an active anti-vibration approach developed based on the principle of similarity as proposed in [13–15], since the NPPF controller possesses the same nonlinearity as the primary structure. Therefore, the optimisation process is sequentially performed in two steps. For step one, the linear version of the NPPF controller i.e. the LPPF controller is optimally configured for a linear single-degree-of-freedom (SDOF) system using the $\mathcal{H}_\infty$ criterion aiming to minimise the maximum steady state response of the primary structure. The derived optimal setting for the LPPF controller serves as a basis for finalising the NPPF controller for vibration mitigation of Duffing oscillators. In step two, the left un-optimised parameter i.e. the coefficient of the cubic term in the NPPF controller is optimally tuned such that the resonance of the Duffing oscillator is damped by the NPPF controller in a similar fashion as that of a linear SDOF system by a LPPF controller for an as large as possible range of excitation levels. For primary systems with other classes of nonlinearities, the corresponding NPPF controller i.e. possessing the same mathematical nonlinear form can be employed and optimised in a similar procedure.

The paper is organised as follows. In the next section, the mathematical model of the system under consideration is first derived, based on which the optimal settings of the LPPF and NPPF controllers are derived using the $\mathcal{H}_\infty$ optimisation criterion. In Section 3, experimental results are presented for the validation of the derived formulae. Conclusions are drawn in Section 4.

2. Mathematical model and H_∞ optimisation

2.1. Modelling

The system under investigation is shown in Fig. 1, which represents a Duffing oscillator. It is defined through a lumped mass m_1, a linear spring k_1 and a cubic spring k_3, and excited by a harmonic force $F = F_d\cos(\omega t)$. A force actuator with its

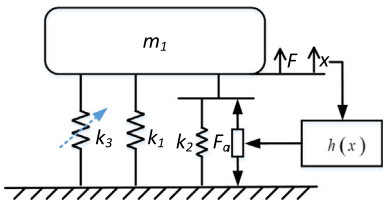

Fig. 1. The schematic of the system under consideration.

stiffness k_2 is placed in parallel to the passive mount. The control loop is implemented by feeding the displacement of the lumped mass $m_1$through a nonlinear controller $h(x)$ to drive the actuator.

The governing equations of the system read:

$$m_1\ddot{x} + k_1x + k_3x^3 = F_d\cos(\omega t) + F_a - k_2x \tag{1}$$

$$F_a = g_1h(x) \tag{2}$$

where F_a is the actuating force proportional to the driving signal, g_1 represents the feedback gain and $h(x)$ is the NPPF control law.

The NPPF controller is designed based on the principle of similarity. A cubic term is thus included in the LPPF controller, which yields:

$$\ddot{u}_a + 2\alpha\omega_f\dot{u}_a + \omega_f^2u_a + \kappa u_a^3 = x \tag{3}$$

where $u_a = h(x)$, α, ω_f and κ are controller parameters.

In order to come to a more general formulation, the following parameters are introduced to normalise the system governing equations:

$$\tau = \omega_1 t,\ \mu = \frac{\omega_f}{\omega_1},\ k_t = k_1 + k_2\ y_1 = \frac{k_tx}{F_d},\ y_2 = \frac{k_t\omega_1^2u_a}{F_d},\ \omega_1 = \sqrt{\frac{k_t}{m}},\ \delta = \frac{k_3F_d^2}{k_t^3},\ g = \frac{g_1}{k_t\omega_1^2},\ \beta = \frac{\kappa k_t}{k_3\omega_1^6} \tag{4}$$

The equations of motion with normalised parameters can then be written as:

$$y_1'' + y_1 + \delta y_1^3 - gy_2 = \cos(\Omega\tau) \tag{5}$$

$$y_2'' + 2\alpha\mu y_2' + \mu^2y_2 + \delta\beta y_2^3 - y_1 = 0 \tag{6}$$

where Ω is the normalised frequency defined as $\Omega = \omega/\omega_1$.

It is shown that the forcing amplitude appears only in the expression of the nonlinear coefficients. The $\mathcal{H}_\infty$ optimisation criterion is employed to optimise the controller $h(x)$ aiming to minimise the maximum magnitude of the frequency response of the system under consideration. In this context, the magnitude of the normalised driving point receptance $|y_1|$ is taken as the performance index.

2.2. $\mathcal{H}_\infty$ optimisation of the LPPF controller

In this subsection, the optimisation of the LPPF controller is performed. This is done by setting the parameter δ in Eq. (5) equal to zero. The normalised driving point receptance of the primary structure is then given by:

$$y_1 = \frac{s^2 + 2\alpha\mu s + \mu^2}{s^4 + 2\alpha\mu s^3 + \mu^2s^2 + s^2 + 2\alpha\mu s + \mu^2 - g} \tag{7}$$

where $s = j\Omega$ is the Laplace variable and the modulus of y_1 is calculated as:

$$|y_1| = \frac{\sqrt{\Omega^4 + (4\alpha^2 - 2)\mu^2\Omega^2 + \mu^4}}{\sqrt{\left(\Omega^2 - 1\right)^2\mu^4 + 2\left((2\alpha^2 - 1)\Omega^4 + (-2\alpha^2 + 1)\Omega^2 + g\right)\left(\Omega^2 - 1\right)\mu^2 + \left(-\Omega^4 + \Omega^2 + g\right)^2}} \tag{8}$$

From the mathematic point of view, the control effectiveness of the LPPF controller according to Eq. (7) would be similar to that of a TMD, where an additional zero is introduced to interfere with the resonance of the primary system aiming to reduce certain vibration metrics in the frequency band of interest. Following the $\mathcal{H}_\infty$ optimisation procedure proposed by Den Hartog [4], the parameters of the LPPF controller are optimally tuned such that the response at the fixed points is minimised. Fixed point refers to the frequency location at which the magnitude of the driving point receptance of the primary structure is invariant in terms of the damping coefficient of the TMD or the parameter α of the LPPF controller.

The frequencies at which the fixed points occur can be calculated by differentiating Eq. (8) with respect to the damping coefficient, α, and equating the derivative to zero, which yields:

$$\Omega_{f1} = \frac{\sqrt{2\mu^2 + 2 - 2\sqrt{\mu^4 - 2\mu^2 + 2g + 1}}}{2} \tag{9}$$

$$\Omega_{f2} = \frac{\sqrt{2\mu^2 + 2 + 2\sqrt{\mu^4 - 2\mu^2 + 2g + 1}}}{2} \tag{10}$$

The optimal μ is set to equalise the resulting performance index as defined in Eq. (8) at the two fixed points. This can be achieved by substituting Eqs. (9) and (10) into Eq. (8) and equating the resulting expressions for $\alpha = 0$, which yields,

$$\mu_{opt} = 1 \tag{11}$$

For the optimal α, it is sought to make the performance index pass horizontally through the fixed points. Thus, two optimal damping coefficients associated with the two fixed points are obtained:

$$\alpha_1 = \sqrt{\frac{3g}{4\sqrt{2}\left(\sqrt{2}-\sqrt{g}\right)}} \tag{12}$$

$$\alpha_2 = \sqrt{\frac{3g}{4\sqrt{2}\left(\sqrt{2}+\sqrt{g}\right)}} \tag{13}$$

The optimal α can be calculated in practice by calculating the quadratic average of Eqs. (12)and (13), which is given by:

$$\alpha_{opt} = \sqrt{\frac{3g}{4(2-g)}} \tag{14}$$

It should be noted that this approach is an empirical method as the resulting resonance points (the derivative of Eq. (8) with respect to Ω is equal to zero) do not necessarily coincide simultaneously with the corresponding fixed points. An exact solution for this problem was proposed in [34], with which the two resulting resonance points are equally mitigated. In this study this exact approach is not considered because this would result in very long and therefore rather impractical polynomial expressions.

Up to now, only the parameter g (normalised feedback gain) is left un-optimised for implementing the LPPF controller. The function of the feedback gain g can be assessed by evaluating the magnitude of driving point receptance at the fixed points. This is done by substituting Eqs. (9) and (11) into Eq. (8) for $\alpha = 0$, which yields the minimal maximum response

$$y_{1\,mm} = \sqrt{\frac{2}{g}} \tag{15}$$

As shown in Eq. (15), the minimal maximum response is inversely proportional to the gain g, indicating that the value of the feedback gain g should be as high as possible without compromising the stability of the active system.

The stability of an active linear system can be studied by applying the Routh-Hurwitz stability criterion to its closed loop characteristic equation [35]. The characteristic equation of the system can be formed as:

$$A_4 s^4 + A_3 s^3 + A_2 s^2 + A_1 s + A_0 = 0 \tag{16}$$

where A_0, A_1, A_2, A_3 and A_4 are the corresponding coefficients of Laplace variable in the denominator of Eq. (7).

The Routh-Hurwitz stability criterion states that the roots of the characteristic equation have negative real parts if and only if the following conditions are satisfied:

$$A_0, A_1, A_2, A_3, A_4 > 0 \tag{17}$$

$$A_2 A_3 - A_1 A_4 > 0 \tag{18}$$

$$A_1 A_2 A_3 - A_1^2 A_4 - A_0 A_3^2 > 0 \tag{19}$$

It can be derived that the system is stable if and only if the gain g is defined such that:

$$g < \mu^2 \tag{20}$$

In the following, numerical studies are performed to illustrate the control effectiveness of the LPPF controller for the system under consideration. Fig. 2 shows the performance index $|y_1|$ plotted against frequency for five different damping ratios defined as α/α_{opt}: 0, 1/4, 1, 4 and ∞, where the control parameters μ is set to its optimal value as given in Eq. (11) and the gain is set to 0.2. It can be seen that all the curves with different damping values intersect at two frequencies and only with the optimal damping the response at the two fixed frequencies becomes maximum. One should also note that the system becomes dynamically softer with the application of the LPPF controller as the control signal is positively proportional to the displacement of the system in the low frequency range where the LPPF control effectiveness is similar to that of a negative spring. However, when the damping value approaches infinity, the softening effect disappears as the control action is lost.

Fig. 3 depicts the performance index $|y_1|$ plotted against frequency for four different feedback gains, namely g: 0, 0.01, 0.05, and 0.5, where the control parameters μ and α are both set to their optimal values. As can be seen, the performance index indeed decreases with an increase in the gain as indicated by Eq. (15). In this respect, the feedback gain g of the PPF controller can be understood to play the same role as the mass ratio between tuned mass dampers and host primary structures, where better performance comes with greater values of this quantity. However, the approximation errors induced by the estimation of the damping parameter α is more pronounced with an increase in the feedback gain. In the

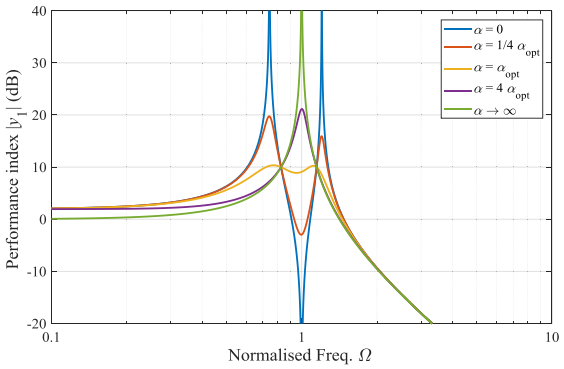

Fig. 2. The driving point receptance for different active damping ratios.

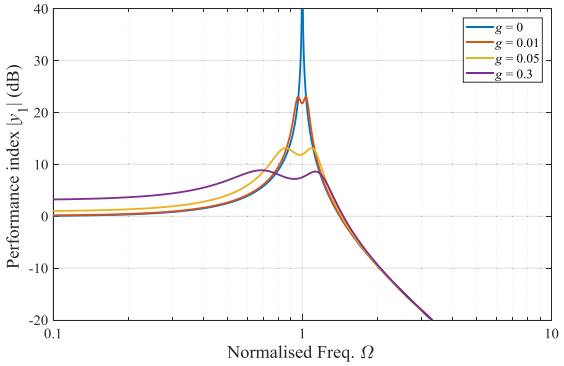

Fig. 3. The driving point receptance for different feedback gains.

same fashion, the response in the low frequency range will be more amplified because of the negative stiffness effect. Therefore, the maximum feedback gain g is not only limited by the stability concern, but also by the amplification of the low frequency response.

2.3. $\mathcal{H}_\infty$ optimisation of the NPPF controller

In this subsection, $\mathcal{H}_\infty$ optimisation of the NPPF controller is performed. Due to the cubic terms, it is difficult to derive the explicit expression of the performance index from Eqs. (5) and (6). As reported in [36–38], harmonic solutions can be used to approximate the exact solutions with a good agreement. In this study, the performance index is approximated using the first-order harmonics. Thus, a one-term harmonic balance approximation is assumed as the solution:

$$y_1 = A_1\cos(\Omega\tau) + B_1\sin(\Omega\tau) \tag{21}$$

$$y_2 = A_2\cos(\Omega\tau) + B_2\sin(\Omega\tau) \tag{22}$$

Substituting Eqs. (21) and (22) into Eqs. (5) and (6), and applying the approximations $\cos^3(\Omega\tau) \approx 3/4\cos(\Omega\tau)$ and $\sin^3(\Omega\tau) \approx 3/4\sin(\Omega\tau)$, a set of polynomial equations is obtained by balancing cosine and sine terms:

$$-A_1\Omega^2 + A_1 - gA_2 + 3/4\delta A_1(A_1^2 + B_1^2) = 1 \tag{23}$$

$$-B_1\Omega^2 + B_1 - gB_2 + 3/4\delta B_1(A_1^2 + B_1^2) = 0 \tag{24}$$

$$-A_2\Omega^2 + 2\alpha\mu\Omega B_2 - A_1 + \mu^2 A_2 + 3/4\delta\beta A_2(A_1^2 + B_1^2) = 0 \tag{25}$$

$$-B_2\Omega^2 - 2\alpha\mu\Omega A_2 - B_1 + \mu^2 B_2 + 3/4\delta\beta B_2(A_1^2 + B_1^2) = 0 \tag{26}$$

Although the original nonlinear differential equations have been transformed to a set of nonlinear algebraic equations, it is not yet possible to find explicit solutions of Eqs. (23)–(26). They are instead solved with approximate solutions. It is further assumed that the nonlinear coefficient δ is a small quantity and the harmonic coefficients A_i and B_i can be expanded into series with respect to the primary nonlinear coefficient δ, i.e. $A_1 = A_{11} + \delta A_{12}$, $B_1 = B_{11} + \delta B_{12}$, $A_2 = A_{21} + \delta A_{22}$ and $B_2 = B_{21} + \delta B_{22}$.

Substituting the above ansatz into Eqs. (23)–(26), collecting the resulting expressions with respect to the order of the parameter δ, and omitting the expressions whose orders are higher than δ^1, one obtains:

$$-gA_{21} - A_{11}\Omega^2 + A_{11} - 1 = 0 \tag{27}$$

$$\frac{(-4\omega^2+4)A_{12}}{4} + \frac{3A_{11}^3}{4} + \frac{3(A_{11}B_{11}^2)}{4} - gA_{22} = 0 \tag{28}$$

$$-gB_{21} - B_{11}\Omega^2 + B_{11} = 0 \tag{29}$$

$$\frac{(-4\omega^2+4)B_{12}}{4} + \frac{3B_{11}^3}{4} + \frac{3(B_{11}A_{11}^2)}{4} - gB_{22} = 0 \tag{30}$$

$$(\mu^2 - \Omega^2)A_{21} + 2\alpha\mu\Omega B_{21} - A_{11} = 0 \tag{31}$$

$$-A_{22}\omega^2 + 2\alpha\mu B_{22}\omega + \frac{3\beta(A_{21}^3 + 3A_{21}B_{21}^2)}{4} + \mu^2 A_{22} - A_{12} = 0 \tag{32}$$

$$(\mu^2 - \Omega^2)B_{21} - 2\alpha\mu\Omega A_{21} - B_{11} = 0 \tag{33}$$

$$-B_{22}\omega^2 + 2\alpha\mu A_{22}\omega + \frac{3\beta(B_{21}^3 + 3B_{21}A_{21}^2)}{4} + \mu^2 B_{22} - B_{12} = 0 \tag{34}$$

Solving for A_{ij} and B_{ij} ($i = 1, 2, j = 1, 2$) from Eqs. (27)–(34), the resulting solutions are found to be in terms of the control gains α, μ, g and the normalised frequency Ω. Due to the complexity, these expressions are not given here. Nevertheless, the modulus of the normalised frequency response $|y_1(\Omega)|$, namely the performance index, can be expressed as:

$$|Q(\Omega)| = \sqrt{A_1^2 + B_1^2} = \sqrt{A_{11}^2 + B_{11}^2 + 2\delta(A_{11}A_{12} + B_{11}B_{12}) + \delta^2\left(A_{12}^2 + B_{12}^2\right)} \tag{35}$$

An additional condition is imposed in order to derive the optimal coefficient of the nonlinear compensator β, which is sought to maintain the equal peaks at the fixed points associated with the LPPF controller for the linear primary system i.e.:

$$|Q(\Omega_{f1})| = |Q(\Omega_{f2})| \tag{36}$$

Substituting the optimal setting of μ and α as given in Eqs. (11) and (14) as well as the solutions of A_{ij} and B_{ij} ($i = 1, 2$, $j = 1, 2$) of Eqs. (27)–(34) into Eq. (36), one obtains

$$\beta_{opt} = 2g - 9/16g^2 + O(g^3) \tag{37}$$

In fact, Eq. (37) represents a simpler and more easily interpretable relation which is the Taylor series expansion of the exact solution (it is not given here either because of the complexity) with respect to the feedback gain g given $g \ll 1$. The relative error introduced by the approximation is fewer than 1.5% up to the dimensionless feedback gain $g = 1$.

Up to now, the derivation of the explicit expressions for forming the NPPF controller $h(\cdot)$ is complete wherein the optimal control parameters μ, α and β are given in Eqs. (11), (14) and (37), respectively. As for the maximum feedback gain g for the NPPF controller, Eq. (20) which constrains the maximum g for the LPPF controller is still applicable according to the Lyapunov's linearisation theory [39]. This theorem states that if the linearised system is strictly stable, then the equilibrium point for the actual nonlinear system is asymptotically stable. It can be proved that the nonlinear system coupled with the NPPF controller as described by Eqs. (5) and (6) can be linearised to the same linear system as described in Section 2.2. However, the Lyapunov's linearisation theory is only valid for small range of motions around the equilibrium points (a local stability theorem) and it is not yet clear what are the boundary conditions for the linearisation approximations to hold (global stability theorem is needed). It is left for the subject of future work.

2.4. Performance of the NPPF controller

Numerical studies are performed to validate and examine the control effectiveness of the NPPF controller for the Duffing oscillator. The performance index derived from the system governing equations given by Eqs. (5) and (6) is computed using a path-following algorithm combining harmonic balance and pseudo-arclength continuation [37]. The first 5 harmonics are

taken for a good approximation and the convergence requirement. The stability of the solutions is determined using Hill's method and the type of instabilities i.e. fold and Neimark-Sacker bifurcations is detected using a test function based on the Floquet multipliers [37]. The 'stability' in the current context is referred to as the local stability of the solutions of the nonlinear equations where the system motion is always bounded. This is different from the concept discussed in Sections 2.2 and 2.3, where the system motion exponentially increases until the system is destroyed if instability happens. In addition, a modal damping of 1% is added to the primary structure during the computation in order to avoid unnecessary numerical errors i.e. infinite-amplitude responses. This particular value is chosen as it also represents the modal damping of the experimental set-up that will be presented in Section 3.

The first study is focused on the validity of Eq. (37) which describes the optimal coefficient of the nonlinear compensator i.e. the cubic term of the NPPF controller. Fig. 4 (a) plots the frequency response of the performance index $|y_1|$ of the Duffing oscillator attached with a NPPF controller whose parameters are configured as follows: the normalised feedback gain g is set to 0.05, the damping ratio and the resonance ratio α and μ are calculated as in Eqs. (14) and (11), respectively, the nonlinear coefficient δ is set to 0.003 and the parameter β varies with respect to its optimal value as β/β_{opt}: 1/4, 1/2, 1, 2 and 4. It is seen that the response at the first resonance frequency increases with an increase of the parameter β and an opposite trend is observed for the second resonance peak. The resonance peaks of equal amplitudes are obtained with the optimal setting of the parameter β as given in Eq. (37). For the parameter setting $\beta/\beta_{opt} = 4$, a pair of fold bifurcations is observed which modifies the stability of the solutions along the frequency response. Fig. 4 (b) compares the performance index of the Duffing oscillator attached with an optimally tuned NPPF controller and its counterpart optimal LPPF controller for the same parameter configuration $g = 0.05$ and $\delta = 0.003$. As can be seen, the LPPF controller is detuned for the system under consideration and a hardening behaviour characteristic of cubic springs with positive coefficients is present at the second resonance peak. On the other hand, the two resonance peaks still remain approximately equal with the NPPF controller which reveals the superior performance of the NPPF controller compared to the LPPF controller.

For the second study, the comparison between the LPPF and NPPF controllers is extended for some other values of the nonlinear coefficient δ which is chosen to vary between 0.0001 and 0.008. Fig. 5 (a) compares the frequency response of the Duffing oscillator with the optimally tuned LPPF controller. As can be seen, when δ is smaller than 0.0008, the LPPF controller works properly, where the responses at the two resonances remain equal and the classical linear results are observed. This is because the input excitation level is not high enough to trigger the nonlinearity of the primary system. However when

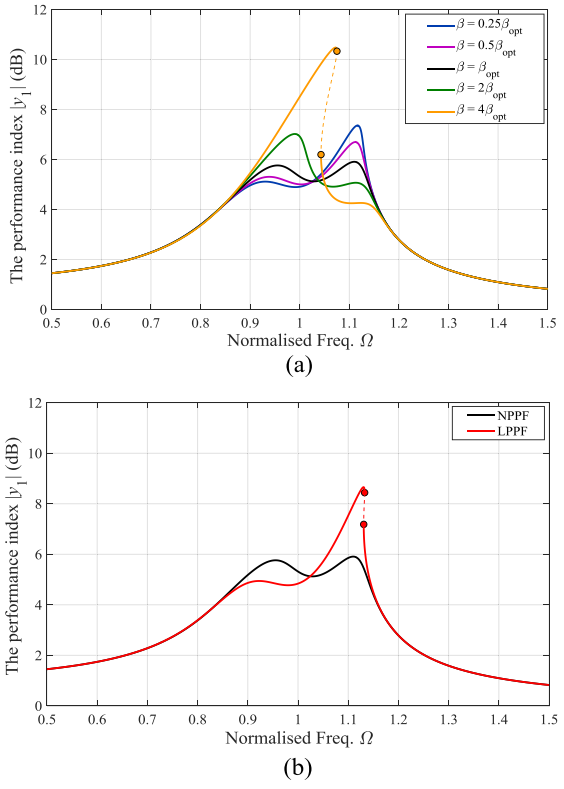

Fig. 4. The performance index $|y_1|$ with the NPPF controller for the feedback gain of 0.05, the primary nonlinear coefficient δ of 0.003 and: (a) different values of the nonlinear coefficient β (b) the optimal nonlinear coefficient β, and comparison with an optimal LPPF controller (—: stable solution, –: unstable solution, ●: fold bifurcation).

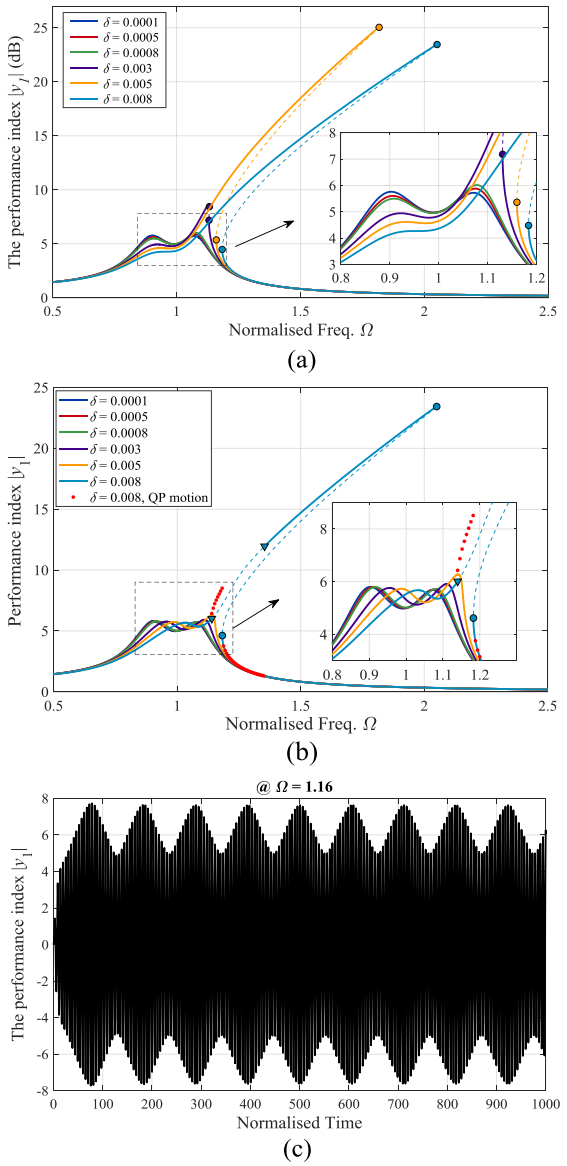

Fig. 5. The performance of the system under consideration where the feedback gain is set to 0.05 and the primary nonlinear coefficient δ varies between 0.0001 and 0.008: (a) with LPPF controller, (b) with NPPF controller and (c) quasiperiodic motion at $\Omega = 1.16$ (—: stable solution, –: unstable solution, ●: fold bifurcation, ▼: Neimark-Sacker bifurcation).

δ is increased to 0.003, a visible difference between the two peak amplitudes is observed, which indicates that the optimal LPPF controller starts to be detuned. Above 0.005, the controller is completely detuned as the response at the second resonance is much greater than that at the first resonance. It is also noted that a sudden shift of the location of the second resonance occurs when δ is increased from 0.003 to 0.005 which is not the case for example when δ is increased from 0.005 to 0.008. This phenomenon is observed because there is an isolated resonance branch, also termed an isola, coexisting with the main frequency response function curve due to the non-uniqueness solutions of nonlinear equations. For $\delta = 0.005$, the isola merges with the main curve at the second resonance leading to a sudden shift of the resonance. On the ground of the observed results, it can be concluded that the LPPF is only effective for weakly nonlinear systems in terms of vibration mitigation.

Fig. 5 (b) depicts the control effectiveness of the optimal NPPF controller for the same system parameter configuration as that applied for the LPPF controller. It shows that the nonlinear controller can compensate LPPF detuning until δ reaches 0.005. However, it is not able to fully eliminate the coalescence of the isola and the main frequency response curve by the proposed NPPF controller as seen for the case when $\delta = 0.008$. This means that the NPPF controller fails to maintain the equal peak property in the presence of a very strong nonlinearity. In addition, another type of dynamical instability

i.e. a pair of Neimark-Sacker bifurcations is observed which leads to a branch of quasiperiodic solutions. The quasiperiodic solutions are computed using direct time integration techniques and the maximum peak amplitude is taken as the response for the plot. It is noted that the quasiperiodic branch suddenly breaks around the first fold bifurcation point and the quasiperiodic solutions after this point merge with the normal oscillation solutions. This indicates that the second half branch of the quasiperiodic oscillations may not be stable i.e. it cannot be physically realised. A time series of the quasiperiodic motions at $\Omega = 1.16$ is plotted in Fig. 5 (c). It is shown that the control performance degrades in the presence of the quasiperiodic motions as the resonance peak is amplified. Nevertheless, the proposed NPPF controller is shown to be able to delay the occurrence of the coalescence of the isola and the main frequency response function curve for relatively large forcing amplitudes compared to the LPPF controller, which also allows to extend the linearity bandwidth of the nonlinear system under control to a relatively large extent. It is foreseen that this bandwidth can be further extended if β is assumed to be also dependent on the nonlinear coefficient δ instead of Eq. (35) which is solely determined by g. This is also left for the subject of future work.

3. Experimental validation

In order to validate the analytical formulae derived for the LPPF and NPPF controllers in Section 2, a representative test bed for a Duffing oscillator was constructed which is shown in Fig. 6. The set-up consists of a cantilever aluminium beam with dimensions 45 cm*3cm*0.3 cm (length*width*thickness), which is clamped at one side and attached with a voice coil actuator (*AVM24-10*) at the other side. Close to the voice coil actuator, an eddy-current sensor was installed to measure the tip displacement of the beam. In this study, only the first bending mode of the beam is considered such that the single mode beam dynamically represents a linear SDOF system. As for the nonlinear cubic spring of the Duffing oscillator, it was realised in an artificial way by feeding back the tip displacement of the cantilever beam through a cubic function to drive the voice coil actuator. With this configuration, it is also possible to simulate nonlinear forces for other applications by applying the corresponding force profiles to the actuator. However, some additional damping is induced due to the installation of the voice coil actuator (the eddy-current effect and air viscous damping effect), which violates the no damping assumption of the primary structure. Thus, a negative damping control loop was implemented in addition in order to eliminate the total inherent damping of the system. This is achieved by calculating the derivative of the tip displacement signal and positively feeding it back to drive the voice coil actuator.

The configuration scheme for the experimental study is depicted in Fig. 7. As seen, the input signal applied to the voice coil actuator comprises four contributions: (i) the disturbance force, (ii) the cubic spring force, (iii) the negative damping force and (iv) the control force. It is noted that the control force delivered by the NPPF controller is calculated in a way similar to that for implementing the 'artificial' Duffing oscillator, where the output of the LPPF compensator is fed through a cubic function and then negatively superposed with the displacement signal (sensor output) in order to form the corresponding nonlinear input signal for the LPPF compensator.

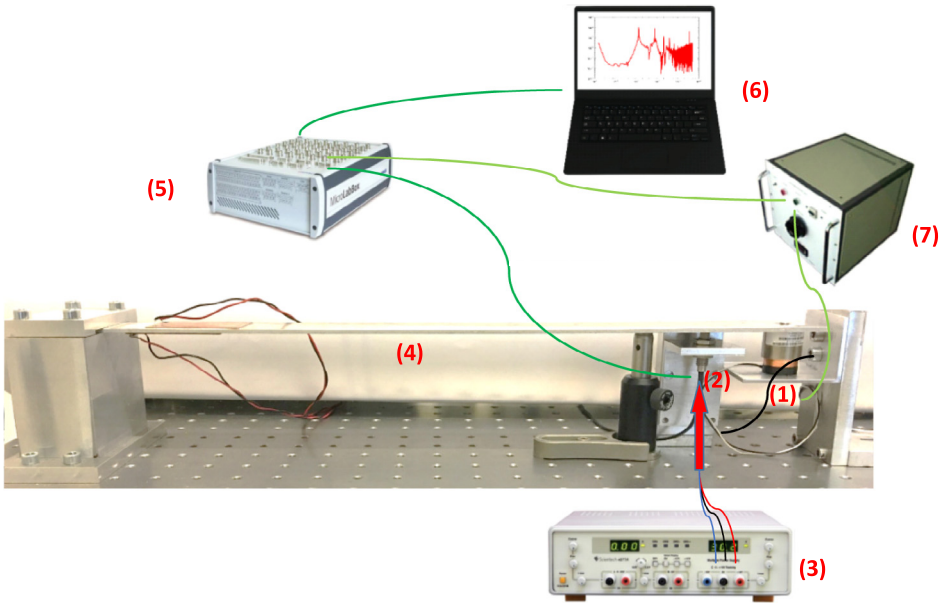

Fig. 6. The experimental test set-up: (1) voice coil actuator, (2) eddy current sensor, (3) DC power source to power the conditioner for the eddy current sensor, (4) cantilever beam, (5) *MicroLabBox*, (6) laptop and (7) current amplifier.

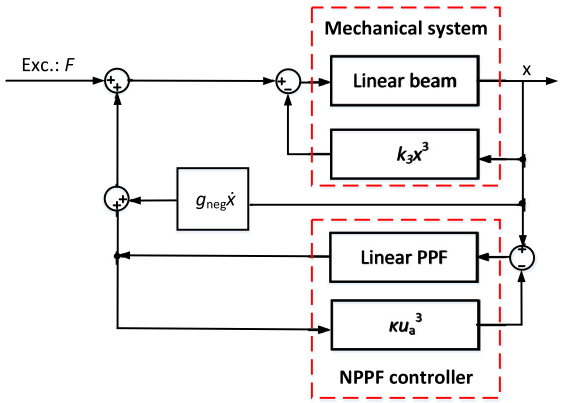

Fig. 7. The configuration scheme for the experimental study.

During the experimental study a *dSpace MicroLabBox* system was used both for data acquisition and for control purposes. The whole control scheme was implemented in the *Matlab Simulink* environment and then downloaded to the processor unit of the *MicroLabBox* system. The control scheme was updated at a sampling frequency of 10 kHz, and the measured data was recorded at the same sampling frequency. A current amplifier (*ADD-45N*) was used to drive the voice coil actuator.

In order to derive the optimal control parameters for the test bed under consideration, system identification was performed. With a curve fitting process, the modal mass, stiffness and the damping ratio (when negative velocity feedback loop is activated) associated with the first bending mode of the cantilever beam were identified; they are given in Table 1. The nonlinear cubic stiffness k_3 was artificially set to 2×10^8 N/m^3.

3.1. Experimental results in a linear regime of motion

The first set of experiments was conducted to test the validity of the optimal control parameters for the LPPF controller. The cubic branches in Fig. 7 for the primary Duffing oscillator and the NPPF controller were deactivated such that the system dynamically behaves in a linear fashion. During the tests, a white noise signal was applied to excite the beam in the vicinity of its first bending motion at 8.6 Hz. The duration of the measurement was set to 200 s. The optimal settings of the LPPF controller are given in Table 1.

Fig. 8 plots the transfer function between the disturbance force and the measured tip displacement, where the parameter α is varied from 1/100 to 100 times the theoretical optimum value. Fig. 9 investigates the effect of the feedback gain g_1 on the frequency response of the driving point receptance, where the parameters α and μ were set to their optimal values as given in Eq. (14) and Eq. (11), respectively. As seen, the obtained experimental results are in accordance with the theoretical analysis. The parameters of the LPPF controller can be tuned to minimise the maximum response of one structural mode in a fashion analogous to that of TMDs. The effectiveness of the LPPF controller at the optimal tuning is also verified to be dependent upon the feedback gain. However, as it was already emphasised in Section 2, the price to pay for this superior performance is the amplification of the response at low frequency. This is because the LPPF controller turns to a proportional controller at low frequency where its control effectiveness is to reduce the effective stiffness of the system thus leading to the low frequency amplification side effect. Figs. 8 and 9 are to be compared with Figs. 2 and 3, respectively.

3.2. Experimental results in a nonlinear regime of motion

The potential of the LPPF and NPPF controllers for damping the Duffing oscillator is experimentally explored in this section. A sine sweep signal is applied as the disturbance to excite the beam. The sine sweep is bounded between 4 and 15 Hz with a sweeping rate of 0.02 Hz/s.

Table 1
Parameters of the Duffing oscillator, optimal LPPF and NPPF controllers, and the level of the excitation force.

Primary system	LPPF	NPPF	Exc. Level
$m_1 = 0.093$ kg	$g_1 = 39,000$ ($g = 0.05$)	$g_1 = 39,000$ ($g = 0.05$)	$F_d = 4$ mN ($\delta = 0.00017$)
			$F_d = 8$ mN ($\delta = 0.00067$)
$k_t = 270.27$ (N/m)	$\mu_{opt} = 1$	$\mu_{opt} = 1$	$F_d = 12$ mN ($\delta = 0.0015$)
$g_{neg} = 0.6$ (damping ratio of 1%)	$\alpha_{opt} = 0.1391$	$\alpha_{opt} = 0.1391$	$F_d = 16.5$ mN ($\delta = 0.003$)
			$F_d = 20$ mN ($\delta = 0.0042$)
$k_3 = 2 \times 10^8$ (N/m^3)		$\kappa_{opt} = 1.8283 \times 10^{15}$ ($\beta_{opt} = 0.099$)	$F_d = 23$ mN ($\delta = 0.0056$)
			$F_d = 27$ mN ($\delta = 0.0077$)

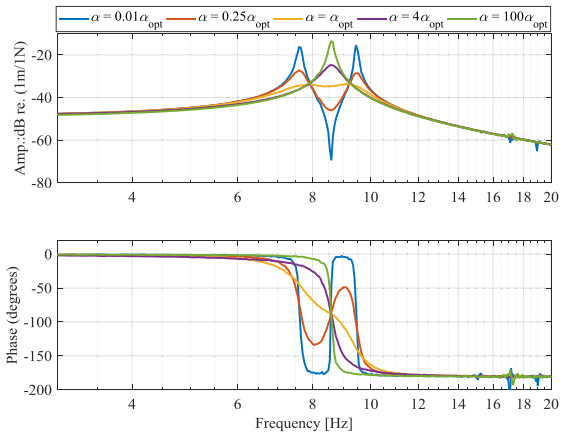

Fig. 8. The frequency response of driving point receptance for different values of the damping ratio α when the LPPF controller is applied.

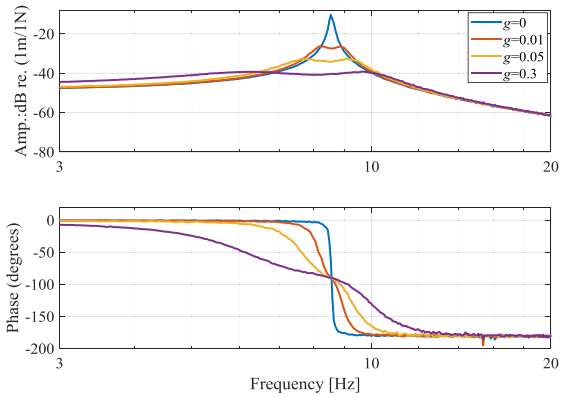

Fig. 9. The frequency response of driving point receptance for different values of the feedback gain g when the LPPF controller is applied.

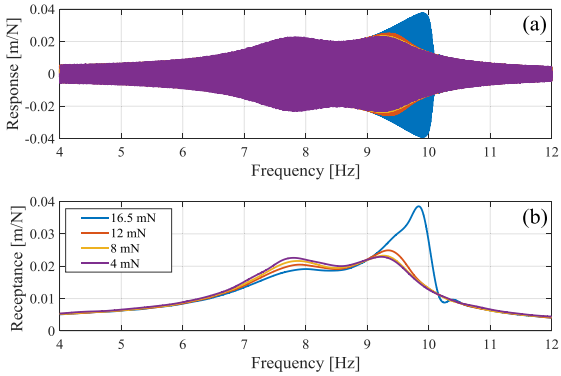

Fig. 10. Measurement of the tip displacement normalised to the excitation level when the LPPF controller is applied: (a) time history signals and (b) its envelope.

The control effectiveness of the LPPF controller for vibration mitigation of the Duffing oscillator is examined first. Fig. 10 (a) plots the time history of the tip displacement normalised to the level of the excitation force which is varied from 4 to 16.5 mN, while Fig. 10 (b) depicts the envelope of the normalised response which thus can be equivalently considered as the driving point receptance, hereafter also referred to as the experimental performance index. The corresponding normalised nonlinear coefficient δ for different levels of the excitation force is calculated according to Eq. (4) and shown in Table 1. As can be seen, the observed experimental results agree well with the theoretical analysis, that is, the LPPF controller

is only effective for weakly nonlinear systems. In addition, a jump phenomenon associated with positive cubic springs is experimentally observed which indicates the existence of the fold bifurcations of the system motion.

Next, the validity of Eq. (37) is experimentally examined by repeating the same tests as conducted for Fig. 4, where the coefficient of the cubic term of the NPPF controller κ is varied over a range from 1/4 to 4 times the theoretical optimum value. The optimal value of κ and its dimensionless counterpart β is given in Table 1. The corresponding experimental results are shown in Fig. 11, which again agree well with the theoretical analysis i.e. the resonance peaks of equal amplitude are obtained with the derived optimal setting of κ.

The control performance of the LPPF and NPPF controllers is experimentally compared for the same feedback gain $g_1 = 39,000$ (normalised gain $g = 0.05$) and the excitation level $F_d = 16.5$ mN ($\delta = 0.003$), which is shown in Fig. 12. It can be seen that the detuned control performance with the LPPF controller in terms of the $\mathcal{H}_\infty$ norm is retrieved by the NPPF controller as predicted in Fig. 4 (b).

The investigation of the NPPF controller is continued with different levels of the excitation force ranging from 8 to 27 mN. The corresponding dimensionless nonlinear coefficient is given in Table 1. The experimental results are presented in Fig. 13 (a) and (b). It can be seen that the control performance with the NPPF controller is maintained for a larger range of excitation force amplitudes compared to the LPPF controller. However, when the disturbance was increased to 27 mN, the response of the system is modulated around 10 Hz, which indicates that the system might fall into the regime of quasiperiodic motions. In order to confirm this, a sinusoidal excitation was used instead, where the frequency varied from 9.7 Hz to 10.2 Hz and the amplitude was set to 27 mN. The evolution of the time series of the normalised system response with respect to the excitation frequency is shown in Fig. 13 (c). It can be seen that the system response below 10.1 Hz exhibits more than one frequency component under a sinusoidal excitation, which is a clear sign of the quasiperiodic oscillations. At 10.2 Hz, the maximum amplitude of the system response suddenly decreases and the quasiperiodic motion disappears. Back to the experimental performance index curve associated with this excitation amplitude as shown in Fig. 13 (b), the results observed can be understood as follows: the system response follows the main frequency response curve until the first Neimark-Sacker bifurcation point located at around 9.7 Hz, then it continues to undergo some quasiperiodic motions between 9.7 Hz and 10.1 Hz and finally the response jumps down to the main frequency response curve instead of continuing to approach the

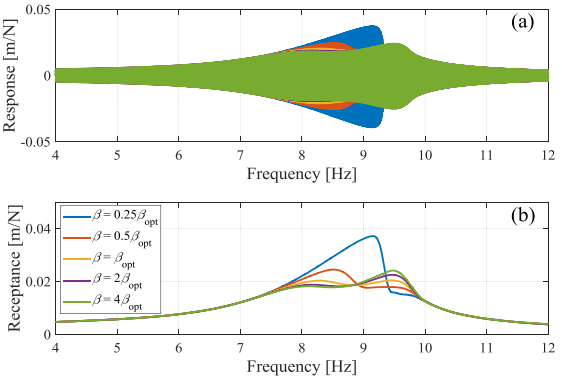

Fig. 11. Measurement of the tip displacement normalised to the excitation level when the NPPF controller with different values of β is applied: (a) time history signals and (b) its envelope.

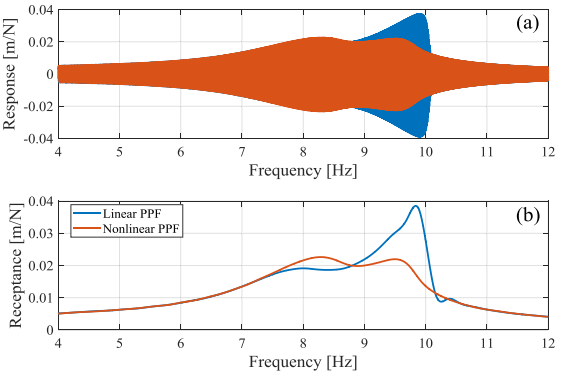

Fig. 12. Experimental performance index obtained with the optimal LPPF and NPPF controllers for the same level of excitation $F_d = 16.5$ mN and feedback gain $g_1 = 39,000$.

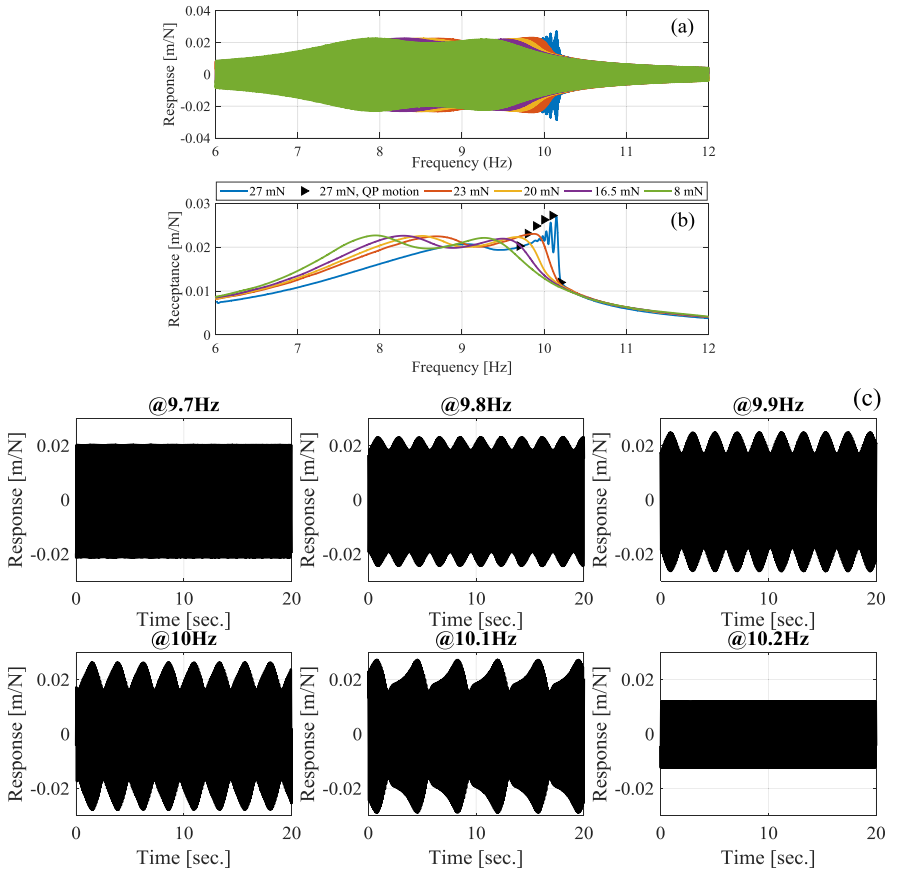

Fig. 13. Measurement of the tip displacement normalised to the excitation level when the optimal NPPF controller is applied: (a) time history signals, (b) its envelope and (c) time series with sinusoidal excitations.

second Neimark-Sacker bifurcation point along the same branch. This trend corresponds well with the numerical investigation as shown in Fig. 5 (b) for the case $\delta = 0.008$.

4. Conclusion

This paper investigates the control effectiveness of a NPPF controller for vibration attenuation of a Duffing oscillator. The proposed NPPF controller is built upon the classical LPPF controller but a cubic term is included according to the principle of similarity. The optimal settings of the LPPF and NPPF controllers are derived using the $\mathcal{H}_\infty$ optimisation criterion. Simple though accurate closed-form expressions are obtained. The harmonic balance method is employed to approximate the analytical solutions, and also to numerically evaluate the proposed tuning methodology. It is shown that the LPPF controller is only effective for weakly nonlinear systems in terms of vibration mitigation, while the NPPF controller could hold the control efficiency for a relatively large range of forcing amplitudes. However, the NPPF controller can be also detuned for very strongly nonlinear regimes. This is because inherently nonlinear dynamical instabilities such as isolas cannot be eliminated by the proposed controller. The analytical study was also validated on an experimental test bed which exhibits the same dynamics as that of a Duffing oscillator. The obtained results correspond well with the theoretical predictions.

Acknowledgements

The financial supports from SPW (Wal'innov 1610122) and F.R.S.-FNRS (IGOR project F453617F) are gratefully acknowledged.

References

[1] F.-Y. Wang, Y. Gao, Advanced studies of flexible robotic manipulators, World Sci. (2003), https://doi.org/10.1142/5290.
[2] M. Darecki, C. Edelstenne, T. Enders, E. Fernandez, P. Hartman, J.-P. Herteman, M. Kerkloh, I. King, P. Ky, M. Mathieu, G. Orsi, G. Schotman, C. Smith, J.-D. Wörner, Flightpath 2050, Flightpath 2050 Eur. Vis. Aviat. (2011) 28. doi: 10.2777/50266.

[3] A.H. Nayfeh, D.T. Mook, Nonlinear Oscillations, Wiley-VCH Verlag GmbH, Weinheim, Germany, 1995, DOI: 10.1002/9783527617586.
[4] J.P. Den Hartog, Mechanical Vibrations, Dover Publications, 1985.
[5] N.W. Hagood, A. von Flotow, Damping of structural vibrations with piezoelectric materials and passive electrical networks, J. Sound Vib. 146 (1991) 243–268, https://doi.org/10.1016/0022-460X(91)90762-9.
[6] G. Zhao, N. Alujević, B. Depraetere, P. Sas, Dynamic analysis and $\mathscr{H}_2$ optimisation of a piezo-based tuned vibration absorber, J. Intell. Mater. Syst. Struct. 26 (2015) 1995–2010, https://doi.org/10.1177/1045389X14546652.
[7] A. Preumont, Vibration Control of Active Structures, Springer, Netherlands, Dordrecht, 2011, DOI: 10.1007/978-94-007-2033-6.
[8] N. Alujević, I. Tomac, P. Gardonio, Tuneable vibration absorber using acceleration and displacement feedback, J. Sound Vib. 331 (2012) 2713–2728, https://doi.org/10.1016/j.jsv.2012.01.012.
[9] N. Alujević, G. Zhao, B. Depraetere, P. Sas, B. Pluymers, W. Desmet, $\mathscr{H}_2$ optimal vibration control using inertial actuators and a comparison with tuned mass dampers, J. Sound Vib. 333 (2014) 4073–4083, https://doi.org/10.1016/j.jsv.2014.04.038.
[10] G. Zhao, G. Raze, A. Paknejad, A. Deraemaeker, G. Kerschen, C. Collette, Active tuned inerter-damper for smart structures and its $\mathscr{H}_\infty$ optimisation, Mech. Syst. Signal Process. 129 (2019) 470–478, https://doi.org/10.1016/j.ymssp.2019.04.044.
[11] G.S. Agnes, R.D. Kriz, Performance of Nonlinear Mechanical, Resonant-Shunted Piezoelectric, and Electronic Vibration Absorbers for Multi-Degree-of-Freedom Structures by Electronic Vibration Absorbers for Multi-Degree-of-Freedom Structures, Virginia Polytechnic Institute and State University, 1997.
[12] M. Febbo, S.P. Machado, Nonlinear dynamic vibration absorbers with a saturation, J. Sound Vib. 332 (2013) 1465–1483, https://doi.org/10.1016/j.jsv.2012.11.025.
[13] G. Habib, T. Detroux, R. Viguié, G. Kerschen, Nonlinear generalization of Den Hartog's equal-peak method, Mech. Syst. Signal Process. 52–53 (2015) 17–28, https://doi.org/10.1016/j.ymssp.2014.08.009.
[14] T. Detroux, G. Habib, L. Masset, G. Kerschen, Performance, robustness and sensitivity analysis of the nonlinear tuned vibration absorber, Mech. Syst. Signal Process. 60–61 (2015) 799–809, https://doi.org/10.1016/j.ymssp.2015.01.035.
[15] G. Habib, G. Kerschen, A principle of similarity for nonlinear vibration absorbers, Physica D 332 (2016) 1–8, https://doi.org/10.1016/j.physd.2016.06.001.
[16] S.S. Oueini, A.H. Nayfeh, J.R. Pratt, A review of development and implementation of an active nonlinear vibration absorber, Arch. Appl. Mech. Ingenieur Arch. 69 (1999) 585–620, https://doi.org/10.1007/s004190050245.
[17] P.F. Pai, B. Wen, A.S. Naser, M.J. Schulz, Structural vibration control using Pzt patches and non-linear phenomena, J. Sound Vib. 215 (2002) 273–296, https://doi.org/10.1006/jsvi.1998.1612.
[18] A. Oveisi, M. Gudarzi, Adaptive sliding mode vibration control of a nonlinear smart beam: a comparison with self-tuning Ziegler-Nichols PID controller, J. Low Freq. Noise, Vib. Act Control. 32 (2013) 41–62, https://doi.org/10.1260/0263-0923.32.1-2.41.
[19] J. Warminski, M.P. Cartmell, A. Mitura, M. Bochenski, Active vibration control of a nonlinear beam with self- and external excitations, Shock Vib. 20 (2013) 1033–1047, https://doi.org/10.3233/SAV-130821.
[20] S.Q. Zhang, Y.X. Li, R. Schmidt, Active shape and vibration control for piezoelectric bonded composite structures using various geometric nonlinearities, Compos. Struct. 122 (2015) 239–249, https://doi.org/10.1016/j.compstruct.2014.11.031.
[21] J. Warminski, M. Bochenski, W. Jarzyna, P. Filipek, M. Augustyniak, Active suppression of nonlinear composite beam vibrations by selected control algorithms, Commun. Nonlinear Sci. Numer. Simul. 16 (2011) 2237–2248, https://doi.org/10.1016/j.cnsns.2010.04.055.
[22] A.T. El-Sayed, H.S. Bauomy, Nonlinear analysis of vertical conveyor with positive position feedback (PPF) controllers, Nonlinear Dyn. 83 (2016) 919–939, https://doi.org/10.1007/s11071-015-2377-6.
[23] W.A. El-Ganaini, N.A. Saeed, M. Eissa, Positive position feedback (PPF) controller for suppression of nonlinear system vibration, Nonlinear Dyn. 72 (2013) 517–537, https://doi.org/10.1007/s11071-012-0731-5.
[24] E. Omidi, S.N. Mahmoodi, Nonlinear vibration suppression of flexible structures using nonlinear modified positive position feedback approach, Nonlinear Dyn. 79 (2015) 835–849, https://doi.org/10.1007/s11071-014-1706-5.
[25] E. Omidi, S.N. Mahmoodi, Nonlinear integral resonant controller for vibration reduction in nonlinear systems, Acta Mech. Sin. 32 (2016) 1–10, https://doi.org/10.1007/s10409-016-0577-z.
[26] E. Omidi, S.N. Mahmoodi, Sensitivity analysis of the nonlinear integral positive position feedback and integral resonant controllers on vibration suppression of nonlinear oscillatory systems, Commun. Nonlinear Sci. Numer. Simul. 22 (2015) 149–166, https://doi.org/10.1016/j.cnsns.2014.10.011.
[27] H. Korschm, H.J. Jodl, T. Hartmann, Chaos, third ed., Springer Berlin Heidelberg, Berlin, Heidelberg, 2008, DOI: 10.1007/978-3-540-74867-0.
[28] I. Kovacic, M.J. Brennan, The Duffing Equation: Nonlinear Oscillators and their Behaviour, John Wiley & Sons Ltd, 2011, DOI: 10.1002/9780470977859.
[29] K. Kecik, Assessment of energy harvesting and vibration mitigation of a pendulum dynamic absorber, Mech. Syst. Signal Process. 106 (2018) 198–209, https://doi.org/10.1016/j.ymssp.2017.12.028.
[30] M. Faghih Shojaei, R. Ansari, V. Mohammadi, H. Rouhi, Nonlinear forced vibration analysis of postbuckled beams, Arch. Appl. Mech. 84 (2014) 421–440, https://doi.org/10.1007/s00419-013-0809-7.
[31] I. Vassilopoulou, C. Gantes, Nonlinear dynamic phenomena in a SDOF model of cable, Arch. Appl. Mech. 82 (2012) 1689–1703, https://doi.org/10.1007/s00419-012-0660-2.
[32] A. Carrella, M.J. Brennan, T.P. Waters, Static analysis of a passive vibration isolator with quasi-zero-stiffness characteristic, J. Sound Vib. 301 (2007) 678–689, https://doi.org/10.1016/j.jsv.2006.10.011.
[33] R.A. Ibrahim, Recent advances in nonlinear passive vibration isolators, J. Sound Vib. 314 (2008) 371–452, https://doi.org/10.1016/j.jsv.2008.01.014.
[34] T. Asami, O. Nishihara, Closed-form exact solution to $\mathscr{H}_\infty$ optimization of dynamic vibration absorbers (application to different transfer functions and damping systems), J. Vib. Acoust. 125 (2003) 398, https://doi.org/10.1115/1.1569514.
[35] L. Meirovitch, Dynamics and Control of Structures, John Wiley & Sons Inc, 1990.
[36] D. Wagg, S. Neild, C.W.S. To, S.K. Lau, Nonlinear Vibration with Control, Springer, Netherlands, Dordrecht, 2010, DOI: 10.1007/978-90-481-2837-2.
[37] T. Detroux, L. Renson, L. Masset, G. Kerschen, The harmonic balance method for bifurcation analysis of large-scale nonlinear mechanical systems, Comput. Methods Appl. Mech. Eng. 296 (2015) 18–38, https://doi.org/10.1016/j.cma.2015.07.017.
[38] G. Kerschen, K. Worden, A.F. Vakakis, J.-C. Golinval, Past, present and future of nonlinear system identification in structural dynamics, Mech. Syst. Signal Process. 20 (2006) 505–592, https://doi.org/10.1016/j.ymssp.2005.04.008.
[39] J.-J.E. Slotine, W. Li, Applied Nonlinear Control, Prentice Hall, Englewood Cliffs, New Jersey, 1991.